Draft version May 27, 2025
Typeset using LaTeX **preprint2** style in AASTeX631

Understanding X-Ray Emission in the Hot CGM

Liam Becker[1]

[1] *University of Washington - ASTR 482*

ABSTRACT

Although the Circumgalactic Medium (CGM) has been thoroughly studied in ultraviolet (UV) wavelengths, high-quality X-ray observations of the CGM are much fewer in number. Recent measurements of the CGM from the eROSITA Final Equatorial Depth Survey find a relationship between stellar mass and X-ray luminosity that conflicts with the IllustrisTNG100 and EAGLE cosmological simulations, indicating the need to incorporate X-ray observations into CGM and galaxy models. In this work, we use a power-law density model to create a parameter space of CGM properties and compute "global" characteristics to determine which combinations of properties can produce a realistic CGM with X-ray emission in agreement with recent observations.

1. INTRODUCTION

The Circumgalactic Medium, or CGM, is a nonuniform, extended structure of gas surrounding galaxies. The CGM acts as an intermediary between gas within galaxies (Interstellar Medium) and gas between galaxies (Intergalactic Medium). Insights into its properties and behavior could lead to a connection between the CGM and galaxy evolution.

Much of the observation and modeling on the CGM has been done in the ultraviolet (UV) wavelengths via the Cosmic Origins Spectrograph (COS) on the Hubble Space Telescope, judging the properties and composition of the CGM from light absorbed by the different ions in the cooler phases of gas ($T \sim 10^4 - 10^5$ K), as in the COS-Halos Survey (Werk et al. 2014). Less often observed, however, is the hot phase ($T > 10^6$ K), where line emission has been predicted (White & Rees 1978; White & Frenk 1991), and more recently, observed (Chadayammuri et al. 2022), which have shown discrepancies between CGM simulations and observations.

The eROSITA Final Equatorial Depth Survey (eFEDS) is a 140 deg^2 field with an almost uniform exposure of roughly 2.5 ks. Chadayammuri et al. (2022) stacked observations of 2643 galaxies in eFEDS in the 0.5–2.0 keV soft X-ray energy band, finding that X-ray luminosity increases more slowly with stellar mass than is predicted by the IllustrisTNG100 and EAGLE cosmological simulations (Schaye et al. 2014; Nelson et al. 2021)—among star-forming and quiescent galaxies alike. Chadayammuri et al. (2022) claim that current simulations and models of galaxies and their CGMs are biased toward the optical and UV observations; in light of their discoveries, these models must be reworked to align with X-ray observation data.

In this work, we use a power-law model to create a parameter space of CGM properties. In Section 2.1 we use a radial density profile to estimate the total mass of a given CGM (2.1.1), the

Corresponding author: Liam Becker
liamb27@uw.edu

bolometric and X-ray emission from the CGM based on cooling data from Cloudy codes (2.1.2 & 2.1.3), and use those estimates to approximate the time for the thermal energy of the CGM to radiate away (i.e. cooling time) (2.1.4). We bound these "global" CGM properties with observations and estimates of reasonable values, using the overlaps of the bounds to constrain our parameter space of CGM properties.

2. METHODS

2.1. *Radial Profiles*

In this work, we use the following radial density profile to define our parameter space:

$$n(r) = n_0 \left(\frac{r}{r_{\rm CGM}} \right)^{-a}. \quad (1)$$

We define $r_{\rm CGM}$ as the outer radius of the CGM, set at the virial radius and ranging from 200–500 kpc; these bounds are derived from the stellar masses used in Chadayammuri et al. (2022) via the stellar mass–halo mass relation (Allen et al. 2019), and scaled by $M_* \propto r_{\rm CGM}^3$. n_0, the particle density of the gas at $r_{\rm CGM}$, is bound from 3×10^{-6} to 1×10^{-4} particles per cubic centimeter. a, the negative slope of our power-law radial density profile is bound from 0.0–2.0; the lower bound is set at 0.0 seeing as density decreases with radius and the upper bound is set at 2.0, the power-law slope of a singular isothermal sphere. Based on Faerman et al. (2017), we assume the CGM to be isothermal, of temperature $T = 1.5 \times 10^6$ K.

2.1.1. *Mass*

We calculate the total mass of a CGM with given values in our parameter space by spherically integrating our density profile from the inner radius of the CGM, $r_{\rm in}$, to the outer radius, $r_{\rm CGM}$, as shown below.

$$M = 4\pi \bar{m} \int_{r_{\rm in}}^{r_{\rm CGM}} n(r) r^2 dr \quad (2)$$

Figure 1 shows contours of constant mass in orange, with boundaries set at 3×10^{10} and 2×10^{11} $M_\odot$, based on the cosmological baryon budget for gas in the CGM (Planck Collaboration et al. 2016).

2.1.2. *Bolometric Emission*

The cooling function gives the bolometric emission of gas in collisional ionization equilibrium (CIE) as a function of temperature and metallicity and is plotted in Figure 2. At lower temperatures ($\sim 10^4$ K), this emission is dominated by H and He line emission, while the bump at intermediate temperatures ($\sim 10^5 - 10^6$ K) is due to line emission in metals, and the tail at temperatures above $\sim 10^7$ K is a result of Bremsstrahlung, or braking radiation (Draine 2011).

Assuming an isothermal hot CGM in CIE with $Z = 0.3$ $Z_\odot$ (Asplund et al. 2009), we took Λ, or the cooling efficiency, to be constant as a function of radius. Using Eq. 3, we calculate the local cooling rate, Γ,

$$\Gamma(r) = \Lambda(T)\ n^2(r). \quad (3)$$

The local cooling rate describes the amount of radiation emitted per unit volume of gas at a certain radius from the center of the galaxy. Multiplying the cooling coefficient (in erg s^{-1} cm^3) by the square of the gas density (in cm^{-3}) results in energy radiated per unit time per unit volume (in erg s^{-1} cm^{-3})—exactly as described.

To calculate the global luminosity of the CGM, we can spherically integrate our radial profiles with Eq. 4.

$$L = 4\pi \int_{r_{\rm in}}^{r_{\rm CGM}} \Gamma(r)\ r^2\ dr \quad (4)$$

2.1.3. *X-Ray Emission*

Since we focus on the X-ray emission of the CGM in this work, we use the Cloudy code to compute cooling coefficient data in the 0.5–2.0

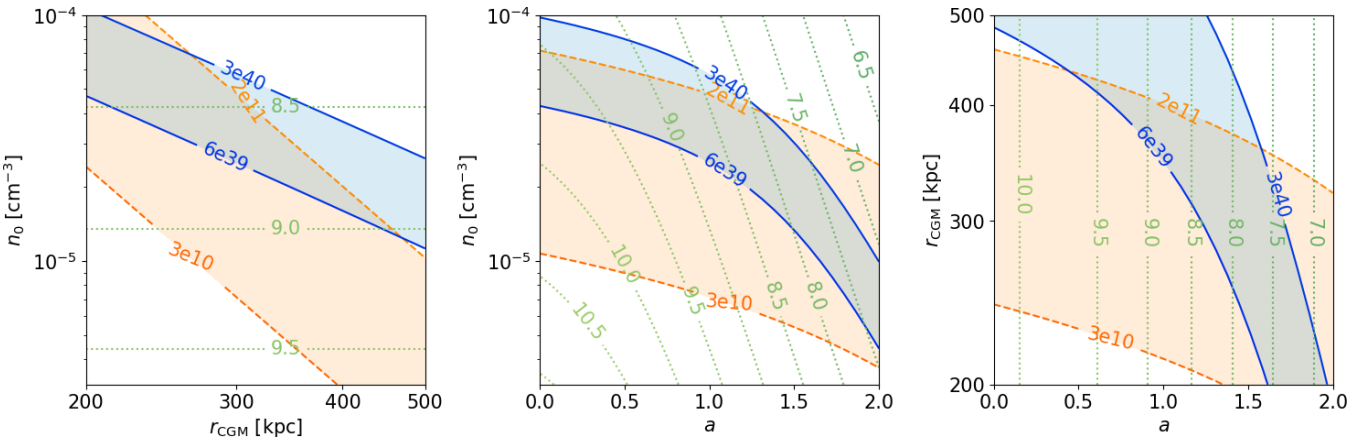

Figure 1. Three slices of our parameter space at $T = 1.5 \times 10^6$ K, showing boundary contours for CGM mass in dashed orange between 3×10^{10} and 2×10^{11} $M_\odot$; luminosity in the 0.5–2.0 keV soft X-ray energy band in solid blue between 6×10^{39} and 3×10^{40} erg s^{-1}; and contours of constant $\log_{10}(t_{\rm cool})$ in dotted green. *Left:* n_0 plotted vs $r_{\rm CGM}$, taking $a = 1.0$. *Center:* n_0 plotted vs a, setting $r_{\rm CGM} = 300$ kpc. *Right:* $r_{\rm CGM}$ plotted vs a, with $n_0 = 2 \times 10^{-5}$ cm^{-3}.

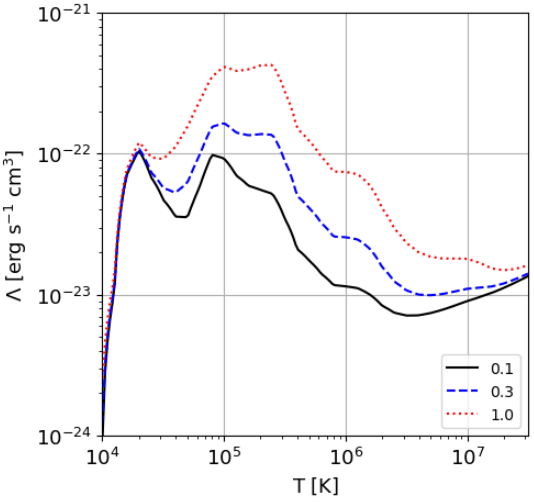

Figure 2. The cooling function plotted at Z = 0.1 (solid black), 0.3 (dashed blue), and 1.0 (dotted red) $Z_\odot$ (Asplund et al. 2009). It can be seen how increasing the metal content of the gas results in stronger metal-line emission in the center of the plot (Draine 2011).

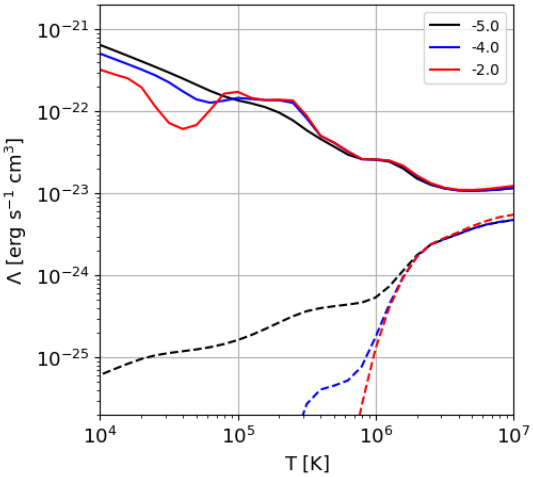

Figure 3. The emission plotted at gas densities of 10^{-5} (black), 10^{-4} (blue), and 10^{-2} (red) cm^{-3}, using data from Cloudy (Ferland et al. 2017; Chatzikos et al. 2023). The solid curves represent bolometric emission, while the dashed curves represent X-ray emission in the 0.5–2.0 keV soft X-ray energy band.

keV soft X-ray energy band as a function of density and temperature, plotted in Figure 3 (Ferland et al. 2017; Chatzikos et al. 2023). We then calculate the local X-ray emission rate, Γ_x, as a function of radius from Eq. 3, for which we numerically integrate via Eq. 4 to find the global X-ray luminosity—blue contours and shaded regions in Figure 1. We place bounds from 6×10^{39} to 3×10^{40} erg s^{-1}, based on the X-ray luminosities measured and plotted in Figure 4 of Chadayammuri et al. (2022), plotted here in Figure 4.

2.1.4. *Cooling Time*

Using the density profiles and assuming an isothermal CGM, we can calculate the thermal energy in the gas with Eq. 5, and integrate to find the total thermal energy of the CGM, as in Eq. 6.

$$E_{\rm th}(r) = 1.5\ k_B\ T\ n(r) \tag{5}$$

$$E_{\rm th,tot} = 4\pi \int_{r_{\rm in}}^{r_{\rm CGM}} E_{\rm th}(r)\ r^2\ dr \tag{6}$$

To estimate the time the CGM would take to radiate away all of its thermal energy, or cooling time ($t_{\rm cool}$), we divide $E_{\rm th,tot}$ by L, as in Eq. 7.

$$t_{\rm cool} = \frac{E_{\rm th,tot}}{L} \tag{7}$$

Contours for $\log_{10}(t_{\rm cool})$ are shown by the green dotted lines in Figure 1. Calculating the cooling time is useful to determine whether a CGM of certain parameters can exist with or without additional heating (e.g. via galactic feedback).

3. DISCUSSION

We find that for an isothermal CGM, the radial density profile in Eq. 1 can reproduce observed X-ray luminosities, as evidenced by the regions of contour overlap in Figure 1. For example, to obtain the necessary emission for a CGM with $r_{\rm CGM}$ of 200 kpc and a negative power-law slope of 1, the left panel shows that the density at $r_{\rm CGM}$ must be quite high to reproduce the X-ray luminosities observed in Chadayammuri et al. (2022). Additionally, the dotted green contours of $t_{\rm cool}$ indicate that such a CGM would radiate its thermal energy in about 1 billion years, meaning that if such a galaxy were observed, there must be heating mechanisms present to support the gas on longer timescales.

In Figure 4 we reproduce Figure 4 from Chadayammuri et al. (2022), plotting X-ray luminosity as a function of $r_{\rm CGM}$. We convert M_* from their plot to $r_{\rm CGM}$ via the method described in Section 2.1—using the stellar mass-halo mass relation and scaling with $M_{\rm halo} \propto r_{\rm CGM}^3$, where $M_{\rm halo} = 10^{12}\ M_\odot$ corresponds to $r_{\rm CGM}$= 255 kpc. We find that varying a, n_0, and T all result in shifts of the lines of calculated luminosity along the y-axis, as is shown for values of a.

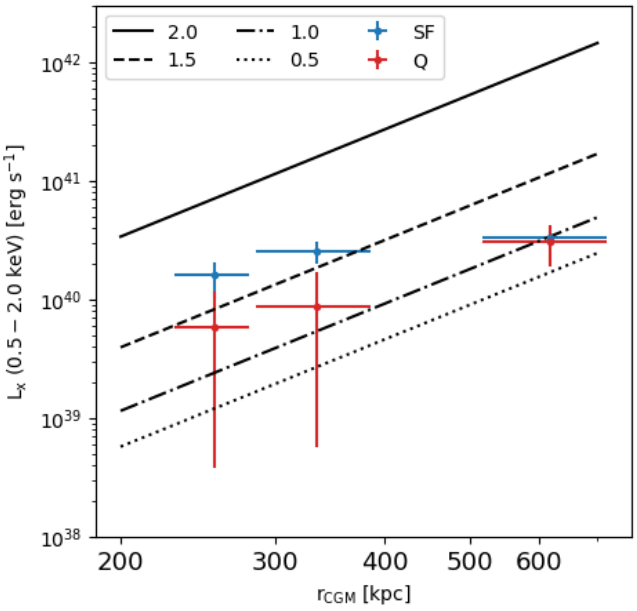

Figure 4. Reproduction of Figure 4 from Chadayammuri et al. (2022)—X-ray luminosity in the 0.5–2.0 keV band as a function of galaxy size (SF for Star-Forming, Q for Quiescent); the x-axis has been changed from M_* to $r_{\rm CGM}$, using the process described in Section 2.1, assuming $M_{\rm halo} = 10^{12}$ $M_\odot$ for $r_{\rm CGM}$= 255 kpc. Additionally, we plot X-ray luminosity, calculated in Section 2.1.3, for n_0= 2×10^{-5} cm^{-3} and a = {2.0, 1.5, 1.0, 0.5}, from top to bottom, respectively.

Although some of the lines intersect the error bars for quiescent galaxies, their slopes are clearly inconsistent with the star-forming ones—this indicates a discrepancy in the relationship between luminosity and $r_{\rm CGM}$ (and M_*, by proxy) in our model. Figure 4 could imply that gas density decreases for larger galaxies (and thus L_x), which may bring our model into

better alignment with the data.

In the future we plan to implement the temperature profiles from Faerman et al. (2020) into our luminosity calculations, seeing as their model better produced other aspects of the CGM. We will also convert our radial luminosity profiles into projected profiles, aiming to compare to the spatially resolved observations in Figure 5 of Chadayammuri et al. (2022), to constrain the slopes and CGM extents in our models. Additionally, we will work to address the difference in the slopes in Figure 4.

APPENDIX

A. PARAMETER SPACE AT MULTIPLE TEMPERATURES

Figure A1 shows plots of the parameter space shown in Figure 1 for temperatures $T = 10^6$, 1.5×10^6, and 2×10^6 K. As temperature increases, the region where M_{halo} and L_x overlap increases as well. Since the CGM is hotter, it takes less density and less volume of gas to reproduce the observed emission, so the L_x contour seems to move "downwards" on the plot.

Logically, increasing temperature increases t_{cool} in kind—if the gas is hotter, there is more thermal energy, thus taking longer to radiate away. This effect can be seen in Figure A1 by the dotted green contours seemingly moving "upwards" in the left panel and "rightwards" in the center and right panels as temperature goes up.

REFERENCES

Allen, M., Behroozi, P., & Ma, C.-P. 2019, MNRAS, 488, 4916, doi: 10.1093/mnras/stz2067

Asplund, M., Grevesse, N., Sauval, A. J., & Scott, P. 2009, ARA&A, 47, 481, doi: 10.1146/annurev.astro.46.060407.145222

Chadayammuri, U., Bogdán, Á., Oppenheimer, B. D., et al. 2022, ApJL, 936, L15, doi: 10.3847/2041-8213/ac8936

Chatzikos, M., Bianchi, S., Camilloni, F., et al. 2023, RMxAA, 59, 327, doi: 10.22201/ia.01851101p.2023.59.02.12

Draine, B. T. 2011, Physics of the Interstellar and Intergalactic Medium

Faerman, Y., Sternberg, A., & McKee, C. F. 2017, ApJ, 835, 52, doi: 10.3847/1538-4357/835/1/52

—. 2020, ApJ, 893, 82, doi: 10.3847/1538-4357/ab7ffc

Ferland, G. J., Chatzikos, M., Guzmán, F., et al. 2017, RMxAA, 53, 385, doi: 10.48550/arXiv.1705.10877

Nelson, D., Springel, V., Pillepich, A., et al. 2021, The IllustrisTNG Simulations: Public Data Release. https://arxiv.org/abs/1812.05609

Planck Collaboration, Ade, P. A. R., Aghanim, N., et al. 2016, A&A, 594, A13, doi: 10.1051/0004-6361/201525830

Schaye, J., Crain, R. A., Bower, R. G., et al. 2014, Monthly Notices of the Royal Astronomical Society, 446, 521–554, doi: 10.1093/mnras/stu2058

Werk, J. K., Prochaska, J. X., Tumlinson, J., et al. 2014, ApJ, 792, 8, doi: 10.1088/0004-637X/792/1/8

White, S. D. M., & Frenk, C. S. 1991, ApJ, 379, 52, doi: 10.1086/170483

White, S. D. M., & Rees, M. J. 1978, MNRAS, 183, 341, doi: 10.1093/mnras/183.3.341

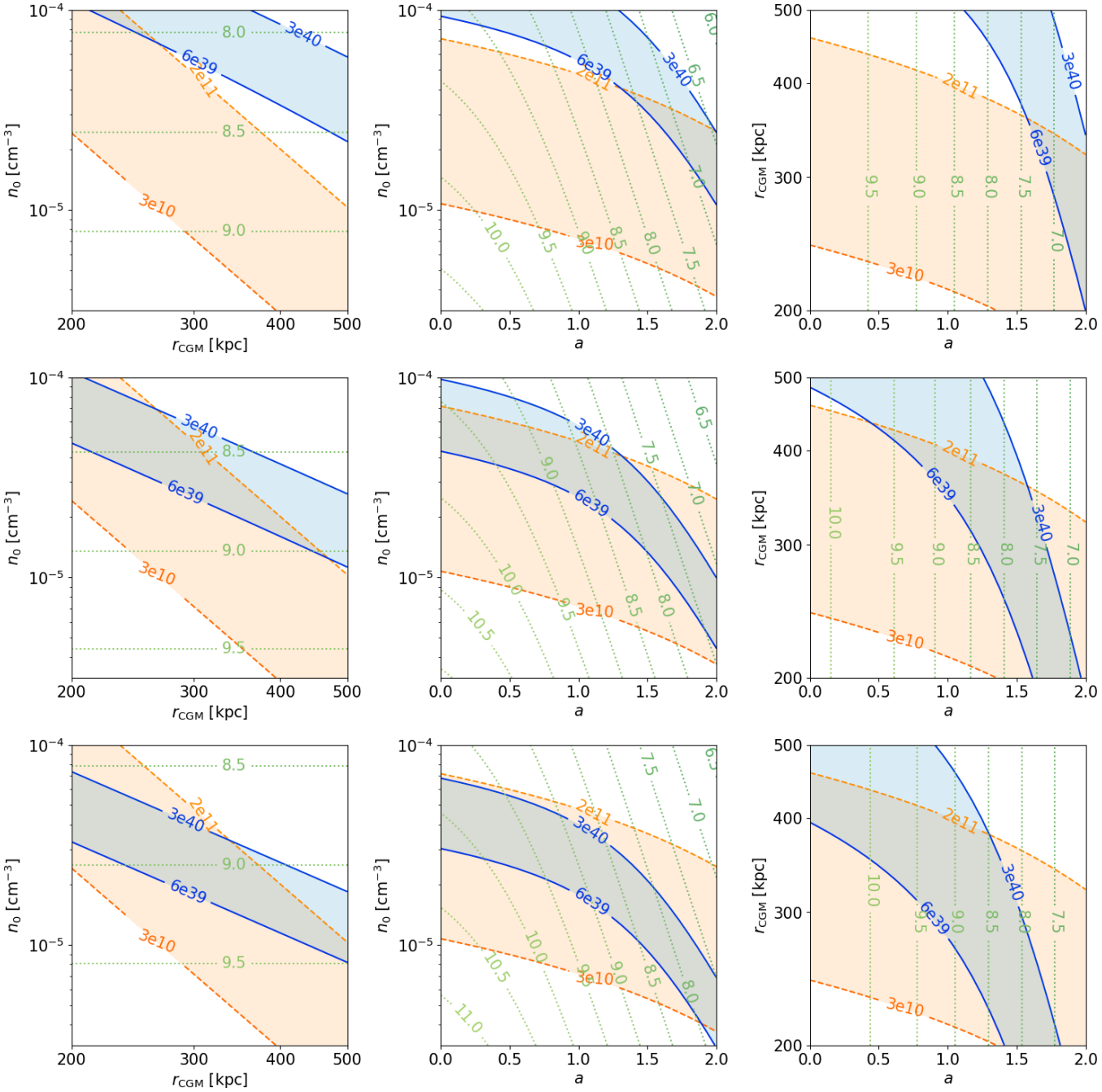

Figure A1. Figure 1 with the temperature set to 10^6 K (*top*), 1.5×10^6 K (*center*), and 2×10^6 K (*bottom*).